Geophysical Research Letters

Supporting Information for

Identification of Repeating Earthquakes:

Misconception of Waveform Similarity and a Physics-based Solution

Dawei Gao[1,2] and Honn Kao[1,2]

[1]School of Earth and Ocean Sciences, University of Victoria, Victoria, British Columbia, Canada

[2]Pacific Geoscience Centre, Geological Survey of Canada, Sidney, British Columbia, Canada

Contents of this file

Texts S1–S3
Figures S1–S11
Tables S1–S3

Introduction

This Supporting Information provides additional texts, figures, and tables to further strengthen the arguments and findings presented in the main text. Texts S1, S2 and S3 describes the technical details of the synthetic experiment setup, the CC calculation, and the DTDD method, respectively. Figure S1 shows an example of synthetic waveforms of both template and matched events for an assumed strike-slip focal mechanism. Figure S2 demonstrates the CC variation as a function of inter-event separation using single-channel waveform data for a normal-faulting focal mechanism. Figures S3 and S4 summarize the testing results of CC variation (obtained with single-station, 3-channel data) due to horizontal and vertical inter-event separations, respectively. Figure S5 illustrates the effects of filtering on CC between non-repeaters (events No. 1 and No. 2) with single-channel data at each station. Figure S6 displays the results of using different window lengths and band-pass filters in determining CC between non-repeaters with single-station (3-channel) data. Figures S7 and S8 illustrate how different band-pass filters could affect waveform similarity at close and distant stations, respectively. Figure S9 demonstrates the effects of window length and filtering in calculating CC between true repeaters (events No. 1 and No. 3). Figure S10 shows the examples of normalized unfiltered waveforms of true repeaters (No. 1 and 3). Figure S11 provides the zoom-in

location map of the Fox Creek events (No. 4-6). Table S1 is a compiled list of different criteria in identifying repeaters. Tables S2 and S3 summarize the commonly used digital filters and commonly assumed stress drop values in previous studies, respectively.

Text S1. Synthetic Experiment Setup

The configuration of our synthetic experiments is shown in Figure 1. Due to the symmetrical setup of our experiment, it is sufficient to focus our investigation on stations in the first quadrant. For the demonstration purpose, we place three stations at the azimuths of 15°, 45°, and 75°, respectively. To explore the effects from various source parameters, we conduct our tests with two different focal depths (D = 3 or 10 km), three representative focal mechanisms (strike-slip, normal, or reverse faulting), and three different epicentral distances (R = 5, 50, or 150 km, Figure 1). In total, 36 scenarios that correspond to either horizontal (±5 km) or vertical (±3 km) inter-event separation are studied in detail. The synthetic seismograms are generated and processed exactly the same way as an earlier study (Gao and Kao, 2020). The details of CC calculation are presented in Text S2.

Text S2. CC Calculation

To calculate the CC value of an earthquake pair, we utilize the recently developed match-filtering with multi-segment cross-correlation (MFMC) technique (Gao and Kao, 2020) instead of the classical cross-correlation method which can be severely biased by the existence of large-amplitude phases such as S wave and surface waves (e.g., Kraft and Deichmann, 2014; Myhill et al., 2011; Li et al., 2017; Gao and Kao, 2020). Compared with the conventional one-segment approach, the MFMC technique splits the template into a number of consecutive segments during the cross-correlation process. Such a procedure is designed to mitigate the impact of the large-amplitude phases and essentially gives more weights to important low-amplitude phases such as depth phases (Ma and Atkinson, 2006; Ma, 2010) and coda waves (Snieder and Vrijlandt, 2005; Robinson et al., 2011) that carry additional source location information. Thus the MFMC technique is more reliably in capturing the waveform discrepancy and differentiating the source location difference between an event pair (Gao and Kao, 2020).

In our MFMC CC calculation, we first cut the waveform from the template event starting at the onset of the P wave with a length of T_{win}. For synthetic experiments, we use a dynamic template window length of $T_{win} = 3(T_s - T_p)$, where T_s and T_p are the S- and P-phase arrival times, respectively. Using a dynamic template window length based on the differential traveltime between P and S phases is necessary to properly account for the increasing wave train with epicentral distance (R = 5, 50, or 150 km in our experiment, Figure 1a) (Baisch et al., 2008; Gao and Kao, 2020). For real earthquake waveform tests in Parkfield area, we tested both dynamic (i.e., $3(T_s - T_p)$) and fixed T_{win} (1.5 s, 3.0 s, 4.5 s, and 6.0 s) for each station given the small study area (Figure 3a). It should be noted that a fixed T_{win} of 6.0 s, equivalent to $12(T_s - T_p)$ of the closest station LCCB (Figure 3a), is sufficiently long covering much of the low-amplitude coda waves. Then the template waveform is divided into N_{seg} segments of equal length. For

unfiltered waveforms, N_{seg} is assigned as 4; for filtered waveforms, the value of N_{seg} is determined by the cycles of the longest period wave ($1/f_{min}$) in the band-pass filtered waveform (i.e., $N_{seg} = T_{win} \times f_{min}$) and the minimum value of N_{seg} is set to be 4 as suggested by an earlier study (Gao and Kao, 2020). At last, all the segments are shifted together one sample point at a time from 0.5 s before the P arrival of the targeted event to 0.5 s after. The cross-correlation calculation is performed individually for each segment, and the CC value at each sample point is given by the average of all segments. The maximum CC value of all time steps is defined as the final CC value of the earthquake pair. If data from three channels of the same station are used, the CC value of all time steps from all three channels are averaged, and the maximum within the sliding window is taken as the final CC.

Text S3. The Differential Traveltime Double-Difference (DTDD) Method

To precisely estimate the relative location between an event pair, we develop the differential traveltime double-difference (DTDD) method which minimizes the residual between observed and predicted relative S-P differential traveltime through three-dimensional (3D) grid search. The relative S-P differential traveltime, ΔSP_{ij}^{k}, between events i and j at station k is given by:

$$\Delta SP_{ij}^{k} = SP_{i}^{k} - SP_{j}^{k} \quad (1)$$

where SP_{i}^{k} and SP_{j}^{k} are the S-P differential traveltimes of events i and j at station k, respectively. If we take the event i as the reference, the relative location of event j is obtained by searching all the possible locations around the reference event in a 3D space. The best location is defined as the grid node which yields the minimum sum of the residuals, R, between observed and predicted relative S-P differential traveltimes:

$$R = \sum_{k} \left| (\Delta SP_{ij}^{k})^{obs} - (\Delta SP_{ij}^{k})^{cal} \right| \quad (2)$$

where $(\Delta SP_{ij}^{k})^{obs}$ and $(\Delta SP_{ij}^{k})^{cal}$ are the observed and theoretical relative S-P differential traveltimes, respectively. Combining (1) and (2) yields:

$$R = \sum_{k} \left| (SP_{i}^{k} - SP_{j}^{k})^{obs} - (SP_{i}^{k} - SP_{j}^{k})^{cal} \right| \quad (3)$$

which is the double-difference of the S-P differential traveltime. It should be noted that, in the measure of misfit (Equations 2 and 3), we use the L1 normal instead of the widely used L2 norm (least squares) because L1 normal is more robust and less sensitive to outliers (Shearer, 1997; Shearer, 2009; Trugman and Shearer, 2017).

When implementing the 3D grid search, we employ a two-step strategy to minimize the calculation, i.e., using a large grid size for initial locating and a very small one for the final solution. Taking the Fox Creek events (No. 4-6) for example, we take the largest event No. 6 as the reference location and define the search volume as the cubic space of 1 km × 1 km × 1 km centred at the reference event. The preliminary solution is determined with a grid search at the spacing of 10 m. Once the preliminary location is identified, we conduct a finer search at the interval of 1 m within the 20 m × 20 m × 20 m cubic space centred at the preliminary solution to obtain the final solution. The effectiveness of our

approach is evident from the located results shown in Figure S11. The hypocentres of both reference (No. 6) and located (No. 4 and No. 5) events generally fall on a line trending N-S, consistent with the inference of a local N-S trending strike-slip fault system (Schultz et al., 2017; Wang et al., 2017).

Compared with the conventional grid search approach which scans all possible locations and origin times to minimize the time residuals between observed and theoretical traveltimes of certain phases (e.g., P and/or S phases; Shearer, 2009), one obvious advantage of the DTDD method is that the relative position is determined without the events' origin times. This formulation effectively avoids the trade-off problem between origin time and source depth. Another added benefit is that it can cancel any path effects due to unmodeled velocity heterogeneities. We note that precise relative location based on the relative S-P differential traveltime can also be solved by conventional inversion schemes (e.g., Cheng et al., 2007). However, the conventional inversion approach may suffer from being trapped to local minima, whereas the forward grid-search approach adopted by the DTDD method always find the global minimum.

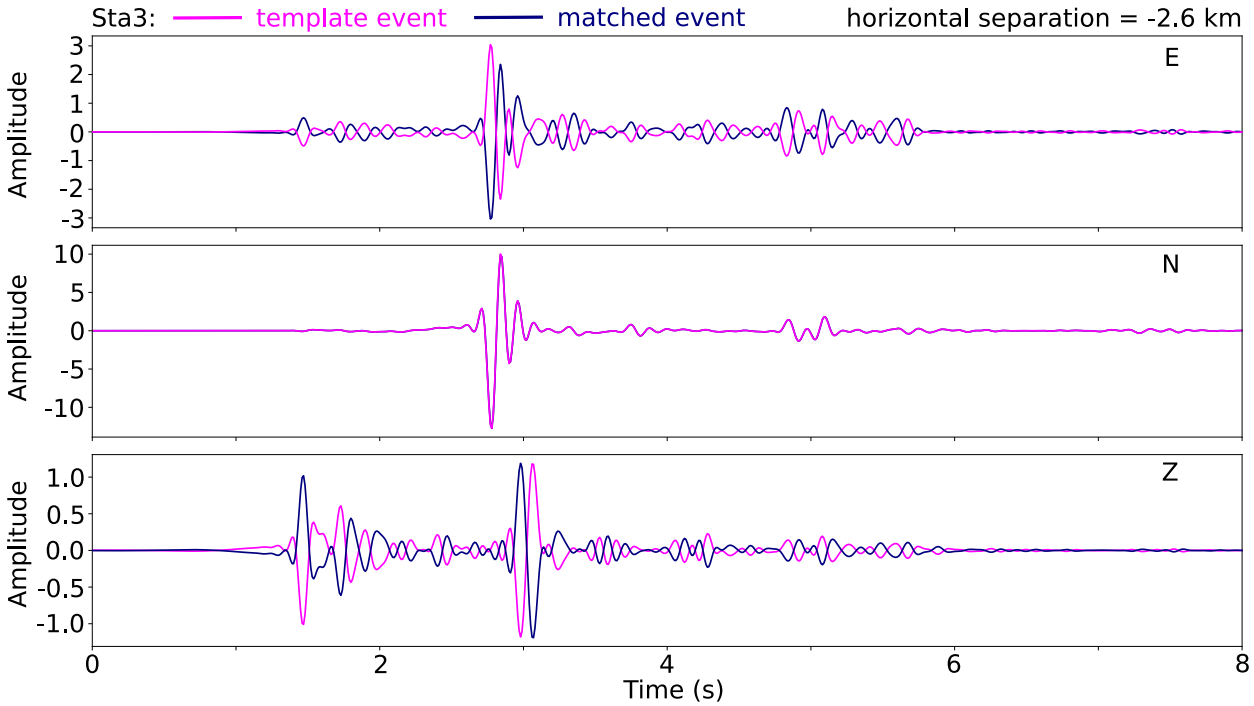

Figure S1. Synthetic waveforms of both template and matched events for a horizontal separation of -2.6 km. The template event is a strike-slip earthquake and is placed at the depth of 3 km. The receiver has an epicentral distance of 5 km with respect to the template event.

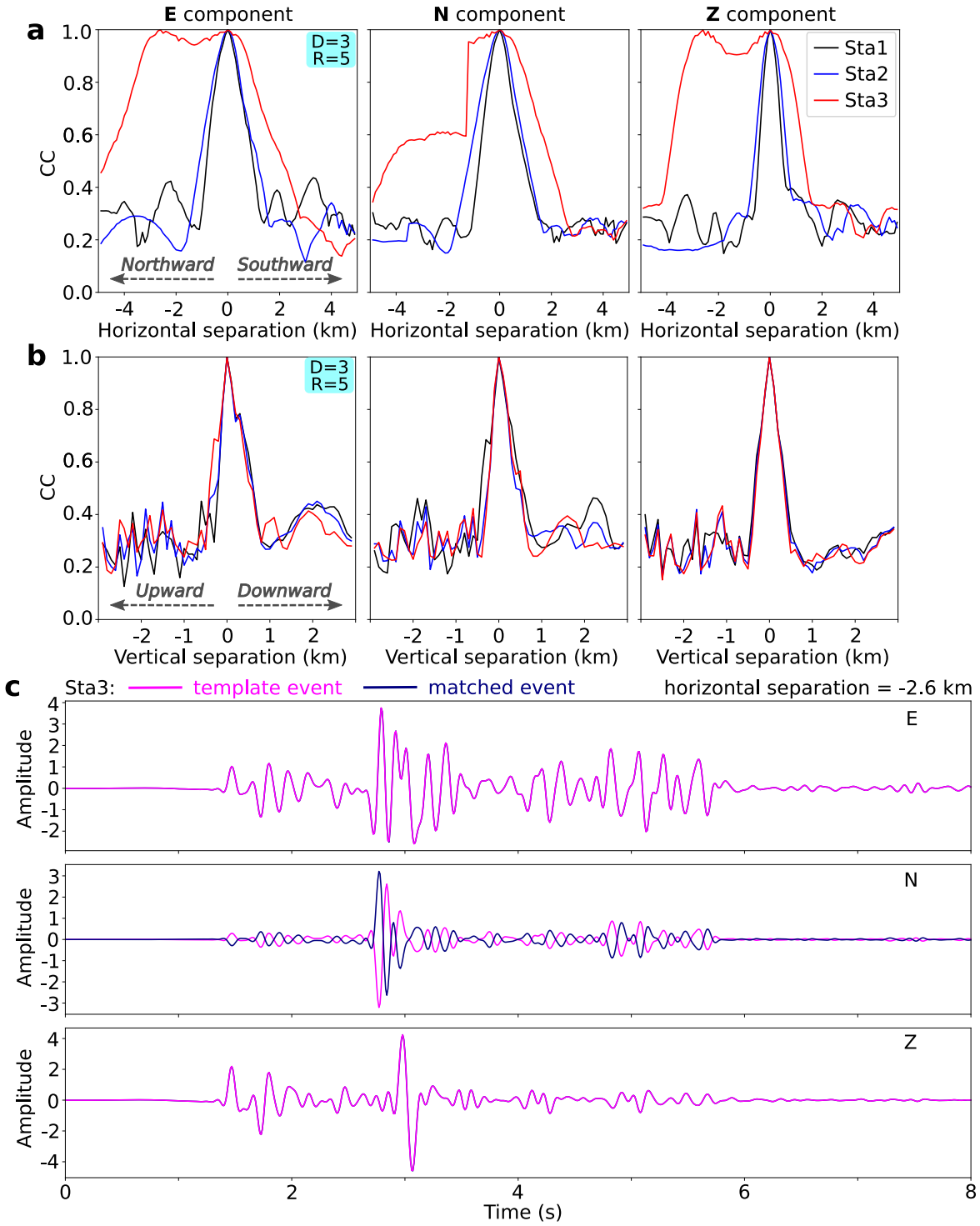

Figure S2. CC variation (obtained with single-channel data) due to inter-event separations. The template event is a normal-faulting earthquake at the depth of 3 km. The receiver has an epicentral distance of 5 km with respect to the template event. (a) CC variation due to horizontal separations. (b) CC variation due to vertical separations. (c) Synthetic waveforms of both template and matched events for a horizontal separation of -2.6 km.

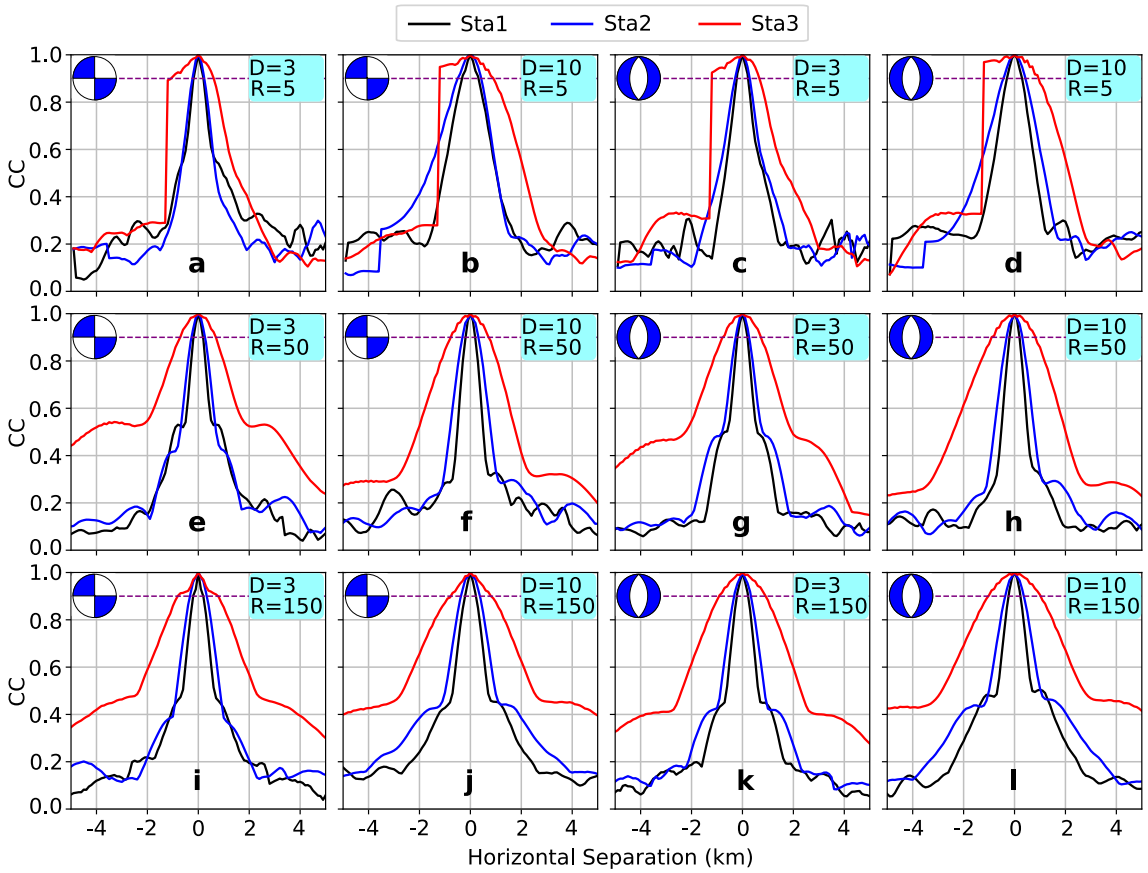

Figure S3. CC variation (obtained with single-station, 3-channel data) due to horizontal inter-event separations. Dashed purple line marks the CC value of 0.90 for reference. Note that the results of a reverse fault are the same as those of a normal fault and hence are not displayed.

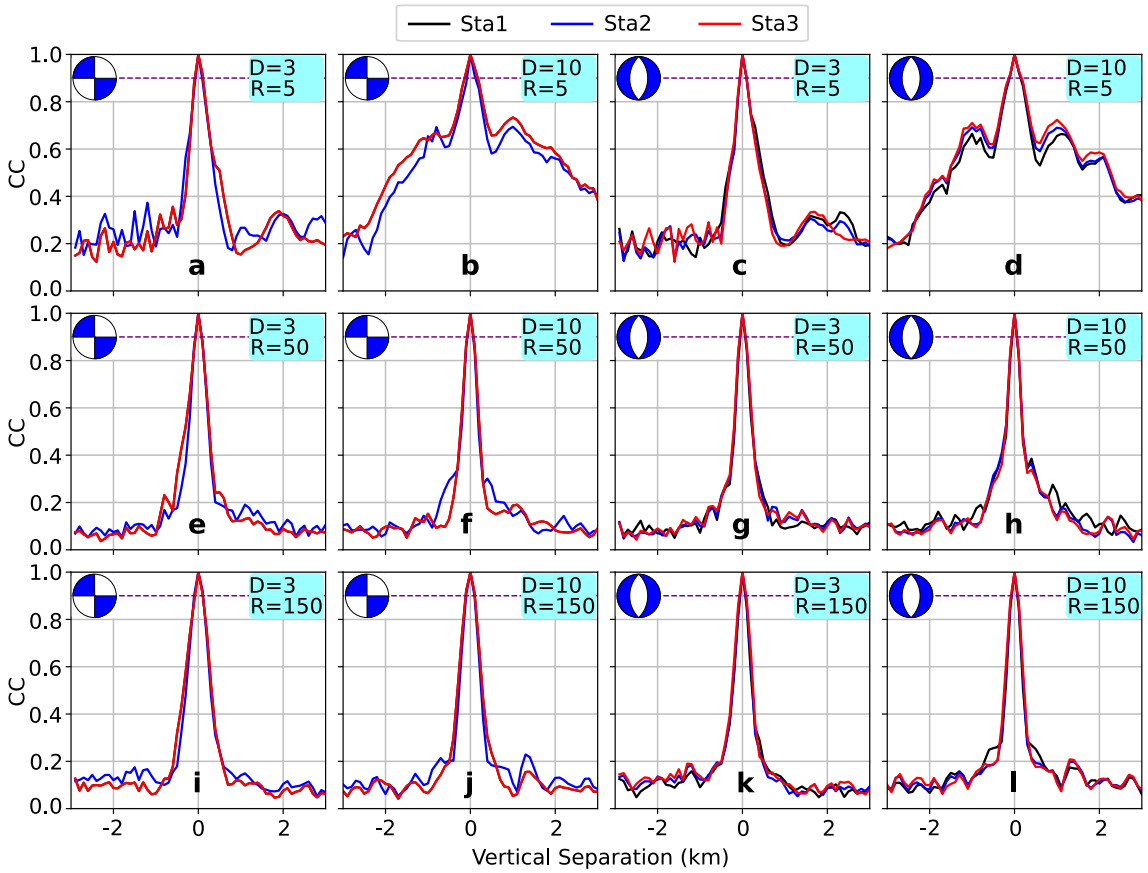

Figure S4. CC variation (obtained with single-station, 3-channel data) due to vertical inter-event separations. Layout is the same as Figure S3. Note that the results of a reverse fault are the same as those of a normal fault and hence are not displayed.

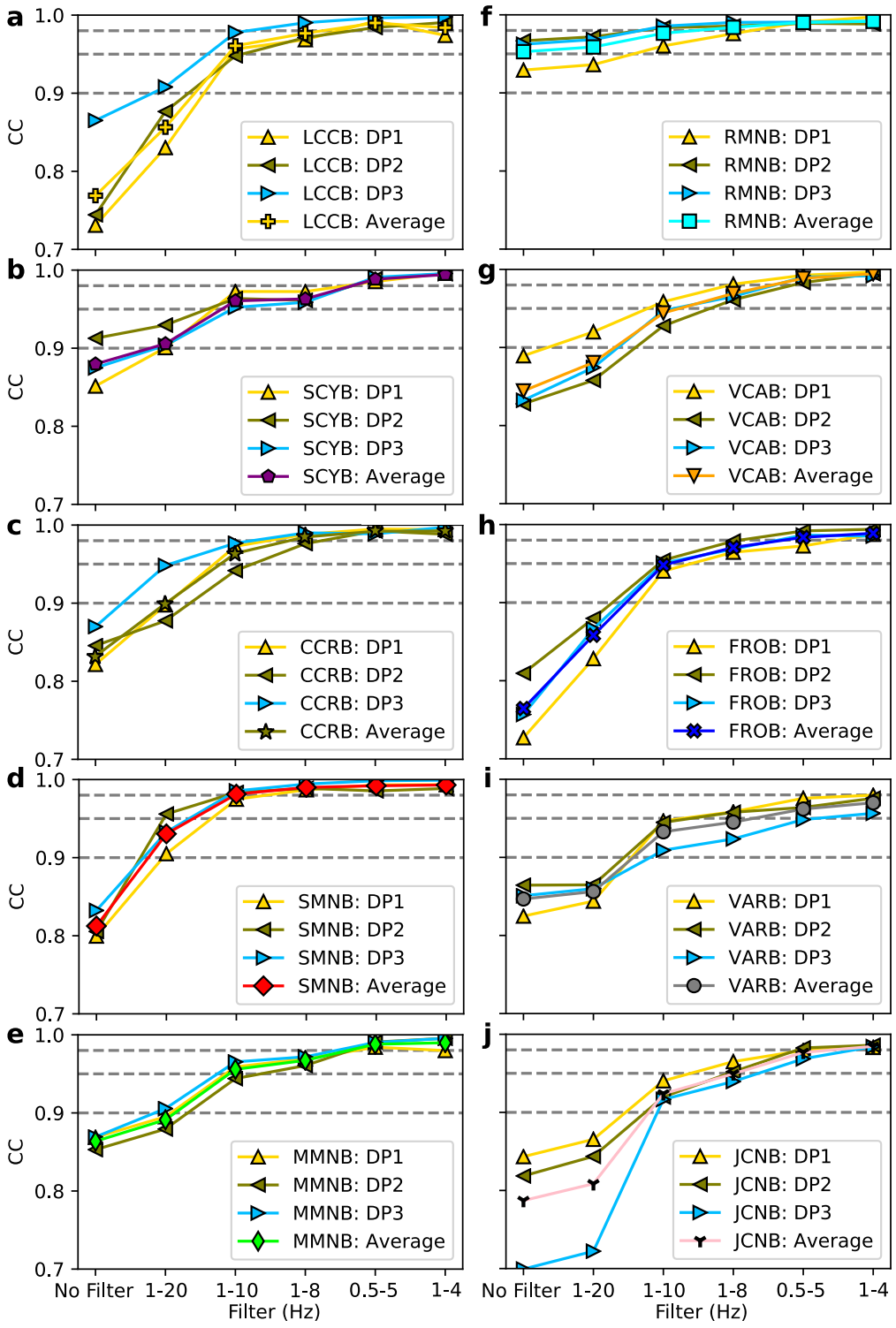

Figure S5. Effects of filtering on the CC value between two events that have been verified to be non-repeaters (events No. 1 and No. 2, Figure 3) with single-channel data. All CC values are determined with the dynamic T_{win} (see Text S2 for more details). For each panel, the station and channel names (e.g., LCCB: DP1) are given in the legend box.

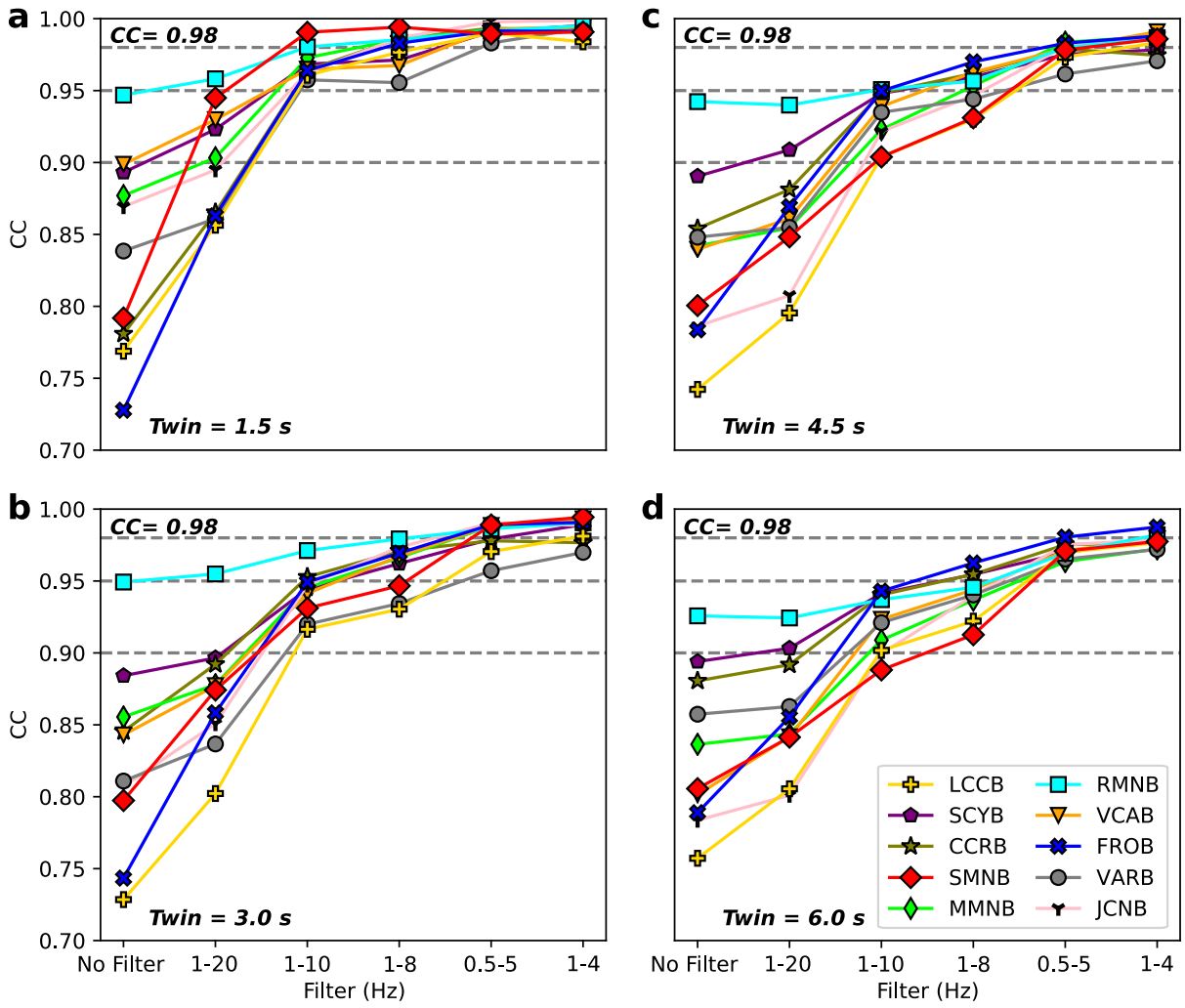

Figure S6. Effects of T_{win} and filtering on the CC value between two events that have been verified to be non-repeaters (events No. 1 and No. 2, Figure 3) with single-station (3-channel) data. (a)-(d) correspond to the T_{win} of 1.5, 3.0, 4.5 and 6.0 s, respectively.

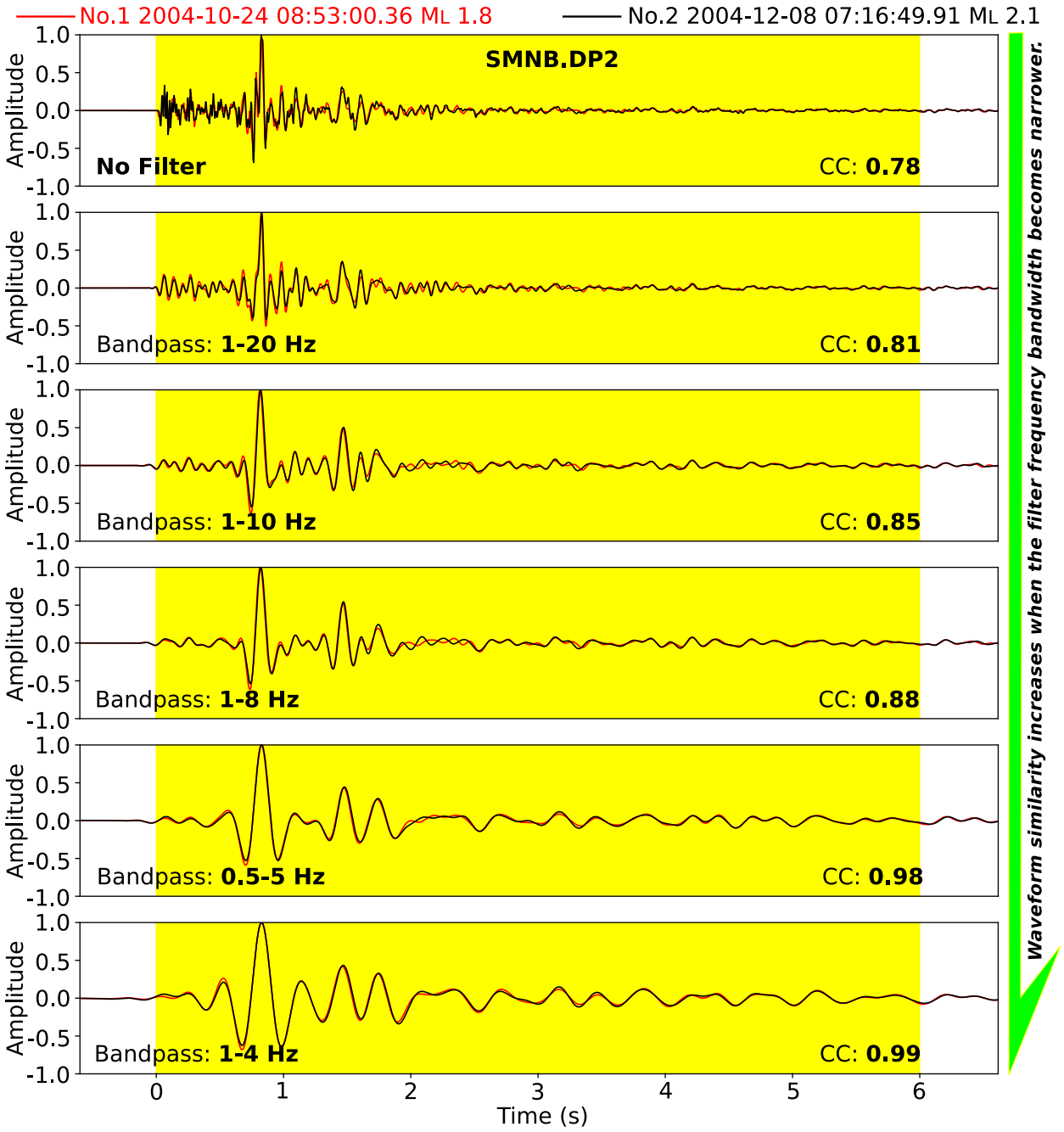

Figure S7. An example of how filtering increases waveform similarity at a close station SMNB. The highlighted segment ($T_{win} = 6.0\ s$) is used to calculate the CC value which is labelled at the lower-right corner. Note that a T_{win} of 6.0 s, equivalent to $10(T_s - T_p)$ at station SMNB, is sufficiently long to cover much of the low-amplitude coda waves.

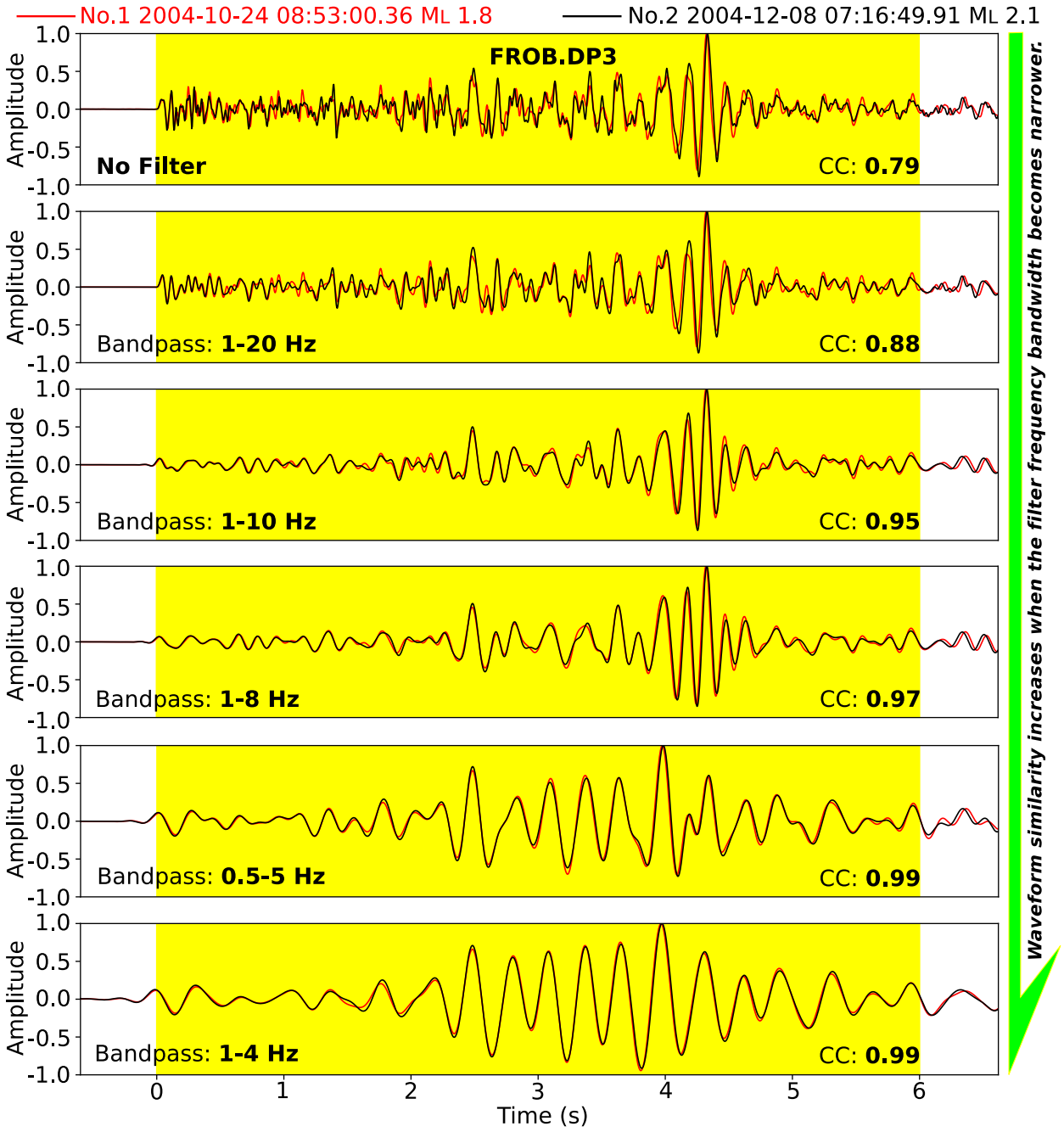

Figure S8. An example of how filtering increases waveform similarity at a distant station FROB. Layout is the same as Figure S7.

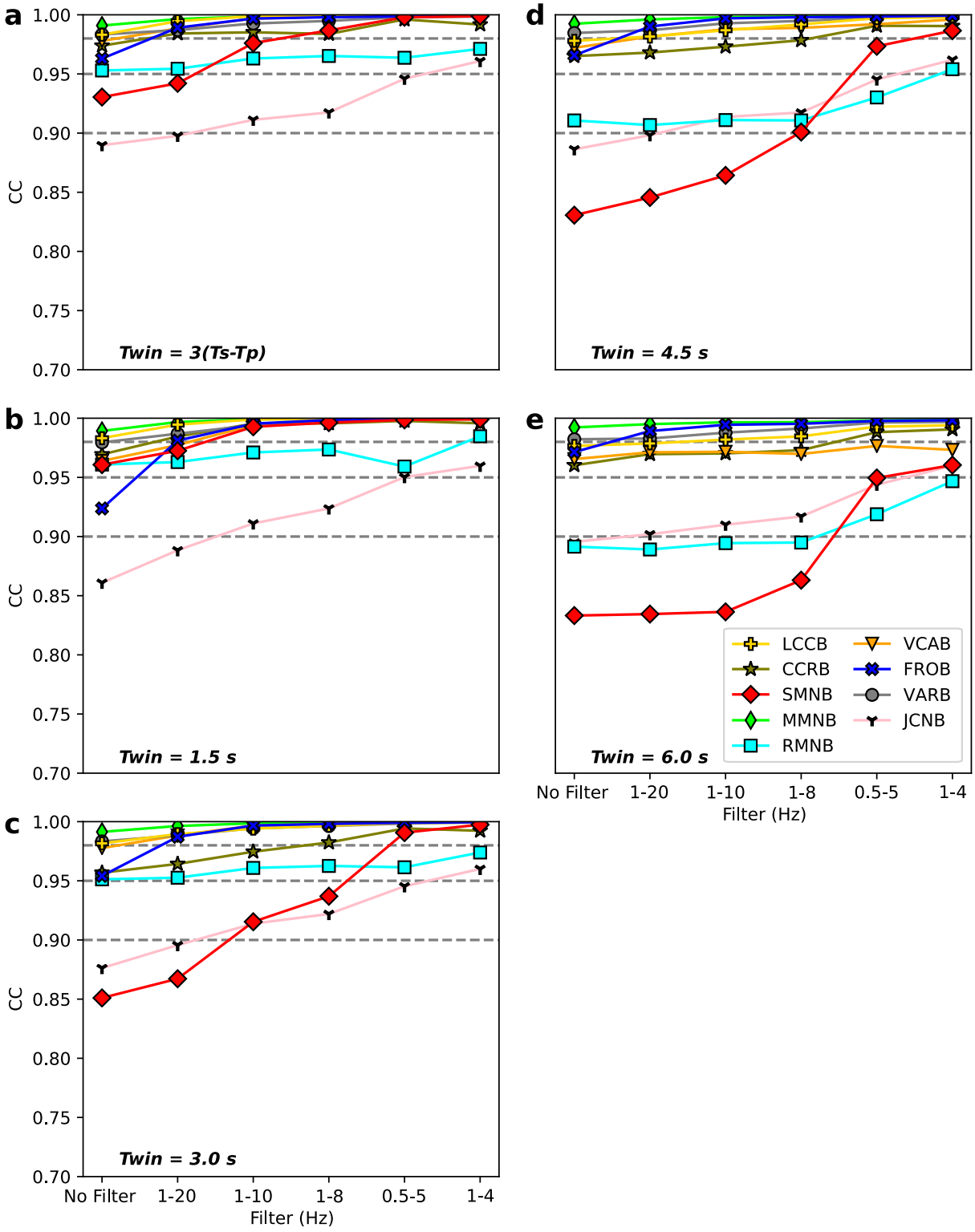

Figure S9. Effects of T_{win} and filtering on the CC value between two events that have been verified to be true repeaters (events No. 1 and No. 3, Figure 3) with single-station (3-channel) data. Notice that station SCYB is not used in this case because of heavy noise contamination. (a) CC determined by T_{win} that is dynamically adjusted for each station. (b)-(d) correspond to the T_{win} of 1.5, 3.0, 4.5, and 6.0 s, respectively.

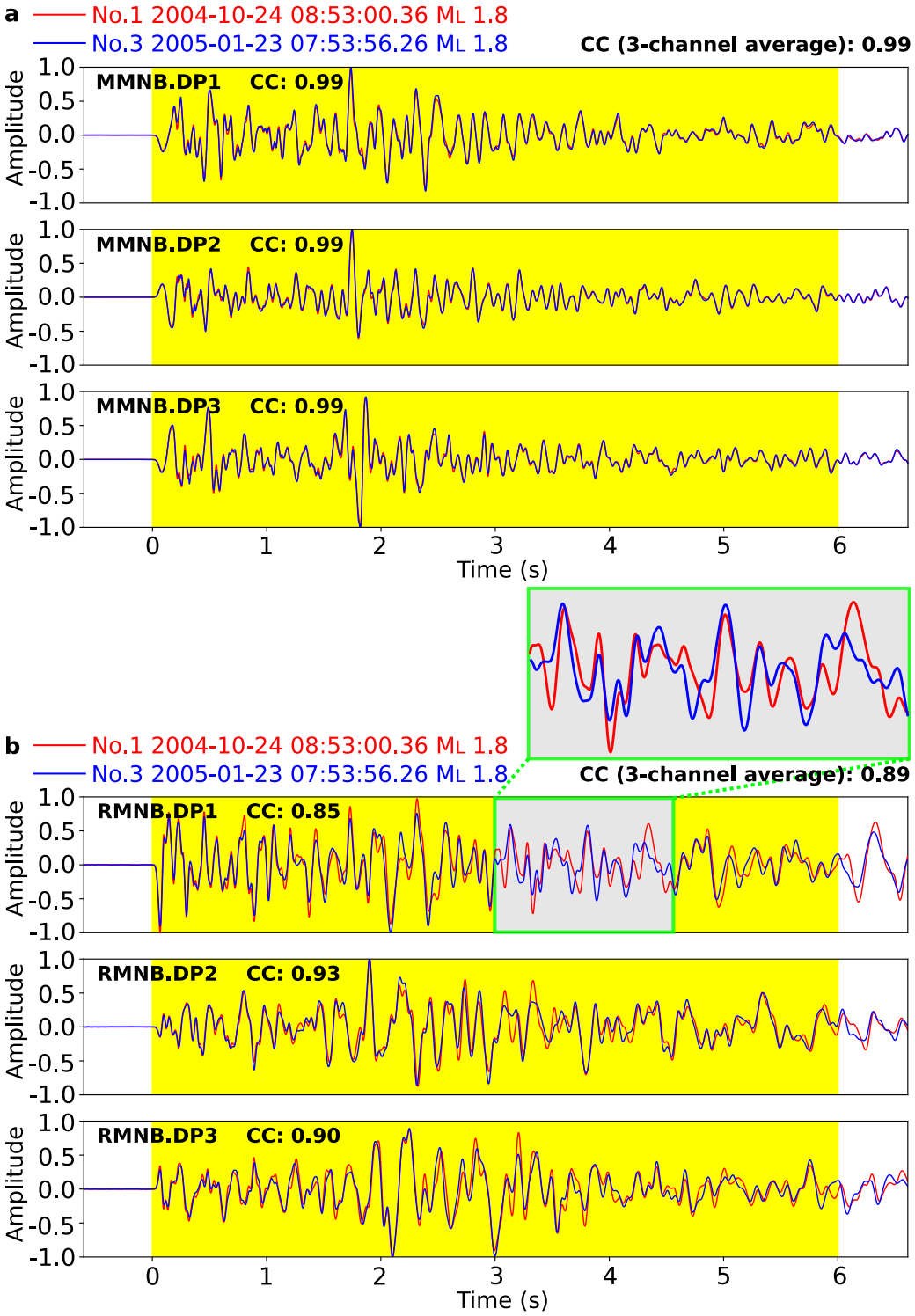

Figure S10. Examples of normalized unfiltered waveforms of two events that have been verified to be true repeaters (events No. 1 and No. 3, Figure 3). (a) Nearly identical waveforms at station MMNB. (b) Waveforms with minor difference at station RMNB. The highlighted segment ($T_{win} = 6.0\ s$) is used to calculate the CC value.

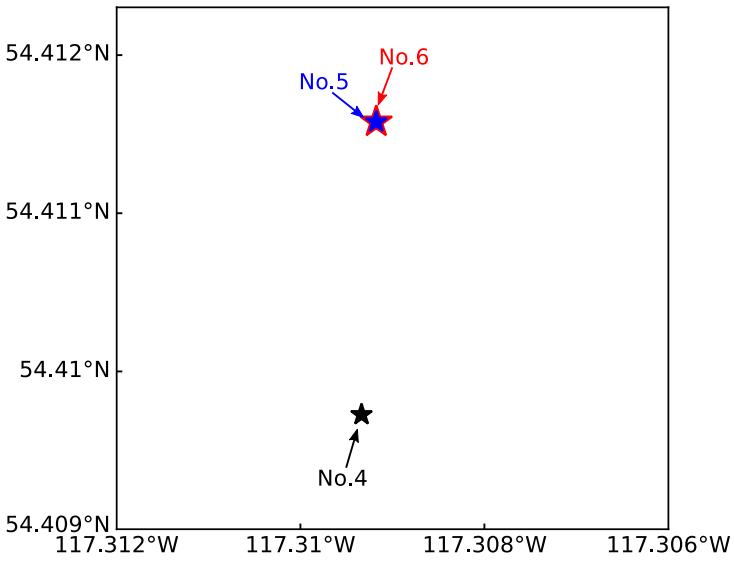

Figure S11. Zoom-in map showing the epicenters of the 3 events in Figure 4.

Table S1. A compiled list of different criteria in identifying repeaters

References	Region	CC Threshold	Additional Criteria/Analysis	Min. Num. of Stations[a,b]	Note
Green and Neuberg (2006)	Soufrière Hills Volcano, Montserrat	0.70		1 station (vertical channel)	
Salvagea and Neuberg (2016)	Soufrière Hills Volcano, Montserrat	0.70		1 station (–)	
Yamada et al. (2016)	Hokkaido, Japan	0.70		1 station (three channels)	
Thelen et al. (2010)	Bezymianny Volcano, Russia	0.70/0.80		2 stations (–)	CC = 0.70 for daily detection; CC = 0.80 for merging results from different days
Thelen et al. (2011)	Mount St. Helens (MSH), Washington; Bezymianny Volcano (BV), Russia	0.70/0.80		2 stations for MSH (–); 2 stations for BV (vertical channel)	CC = 0.70 for daily detection; CC = 0.80 for merging results from different days
Rau et al. (2007)	Longitudinal valley fault, Taiwan	0.70/0.85	composite selection criteria (both CC and S-P differential time)	multi-station (vertical channel)	
Chen et al. (2008)	Chihshang fault, TaiWan	0.70/0.85	composite selection criteria (both CC and S-P differential time)	multi-station (vertical cahnnel)	
Buurman et al. (2013)	Redoubt Volcano, south-central Alaska	0.75		1 station (single-channel)	
Schultz et al. (2014)	Alberta, Canada	0.75		1 station (–)	
Cauchie et al. (2020)	Soultz-sous-Forêts, France	0.75	overlap of rupture areas (inter-event distance < the	1 station (vertical channel)	

			sum of event pair radii)		
De Angelis and Henton (2011)	Soufrière Hills Volcano, Montserrat	0.75		3 stations (–)	
Zhang et al. (2005)	South Sandwich Islands region	0.79			
Schaff and Richards (2004)	China	0.80		1 station (BHZ channel)	
Schaff and Richards (2011)	in and near China	0.80		1 station (BHZ channel)	
Buurman and West (2010)	Augustine Volcano, Alaska	0.80		1 station (vertical channel)	
Petersen (2007)	Shishaldin Volcano, Alaska	0.80		1 station (vertical channel)	
Cannata et al. (2013)	Mt. Etna volcano, Italy	0.80		1 station (vertical channel)	
Li and Richards (2003)	South Sandwich Islands region	0.80		1 station (vertical channel)	visually check waveform similarity
Ma and Wu (2013)	Longmen Shan Fault Zone, China	0.80		1 station (three channels)	
Ma et al. (2014)	Longmen Shan Fault Zone, China	0.80		1 station (three channels)	
Nadeau and McEvilly (2004)	San Andreas Fault	0.80	cross-coherence, visual inspection, relocation, arrival time analysis		CC = 0.80 is used for preliminary scanning
Yu (2013)	Tonga-Kermadec-Vanuatu	0.80	entirely overlapping source areas and similar seismic moment	5 stations (vertical channel)	
Li et al. (2007)	Tangshan fault, China	0.85	average recurrence	1 station (–)	

			interval >100 days; internal consistency of travel time picking; relocation		
Zhang et al. (2008)	South Sandwich Islands, Aleutian Islands, Kuril Islands, Tonga–Fiji–Solomon Islands, Bucaramanga earthquake nest	0.90		1 station (vertical channel)	visually check waveform similarity
Li et al. (2011)	Longmen Shan fault zone, China	0.90	average recurrence interval >100 days; internal consistency of travel time picking; relative distance < rupture sizes	1 station (–)	
Cociani et al. (2010)	Gulf of Corinth, Greece	0.90	inter-event overlap confirmed by relocation and source dimension estimation	1 station (–)	
Hayward and Bostock (2017)	Queen Charlotte plate boundary, Canada	0.90	inter-event overlap suggested by conda wave interferometry	1 station (three channels)	
Bohnhoff et al. (2017)	Marmara, Turkey	0.90	recurrence time > 30 days; hypocentres ≤ 5 km epicentral distance; magnitude difference ≤ ±0.2	2 stations (vertical channel)	

Naoi et al. (2015)	Cooke 4 mine, South Africa	0.90	inter-event separation < half of the rupture radius of the larger event	2 stations (single channel)	
Yamaguchi et al. (2018)	Cooke 4 mine, South Africa	0.90	inter-event separation < half of the rupture radius of the larger event	3 stations (single channel)	
Schmittbuhl et al. (2016)	Main Marmara Fault, Turkey	0.90	confirm overlapping with waveform stretching and spectral analysis	1 station (vertical and horizontal channel)	
Zhao and Peng (2009)	Calaveras fault, California	0.90	magnitude difference < 1; 50% overlaping of the rupture area	3 stations (vertical channel)	CC threshold is the median value at ≥ 3 stations
Meier et al. (2004)	Hellenic subduction zone	0.90		3 stations (–)	
Yao et al. (2017)	Nicoya Peninsula, Costa Rica	0.90	overlap of source area	9 channels	Network-averaged CC
Huang et al. (2020)	Ridgecrest, California	0.90	magnitude difference < 0.5; 50% overlaping of the rupture area; horizontal location error < 0.3×source radius	6 stations (vertical channel)	
Obana et al. (2003)	western Nankai Trough, Japan	0.93/0.95		2 stations (vertical channel)	
Shirzaei et al. (2013)	Hayward fault, California	0.95	coherency > 0.95	1 station (vertical channel)	
Peng and Ben-Zion (2005)	Karadere-Düzce branch of the North Anatolian Fault, Turkey	0.95			

Igarashi et al. (2003)	northeastern Japan	0.95		2 stations (vertical channel)
Uchida et al. (2003)	northeastern Japan	0.95		2 stations (vertical channel)
Matsuzawa et al. (2004)	east off northern Honshu, Japan	0.95		2 stations (vertical channel)
Kimura et al. (2006)	Kanto, Japan	0.95		2 stations (–)
Igarashi (2010)	Japan	0.95		2 stations (vertical channel)
Yamashita et al. (2012)	southwestern Japan	0.95		2 stations (vertical channel)
Kato and Igarashi (2012)	Tohoku, Japan	0.95		2 stations (–)
Kato et al. (2012)	Tohoku, Japan	0.95		2 stations (–)
Meng et al. (2015)	Northern Chile	0.95		2 stations (vertical channel)
Huang and Meng (2018)	central Chile	0.95	magnitude difference ≤ 0.5; stations span a distance > 50 km	2 stations (vertical channel)
Taira et al. (2014)	San Juan Bautista, San Andreas fault	0.95	phase coherency ≥ 0.95	2 stations (vertical channel)
Nishikawa and Ide (2018)	Ibaraki-Oki, Japan	0.95	magnitude difference ≤ 0.5	2 stations (three channels)
Igarashi (2020)	Japan	0.95	composite selection criteria (both CC and S-P differential time)	2 stations (vertical channel)
Matsubara et al. (2005)	northern Japan	0.95		3 stations (vertical channel)
Kato and Nakagawa (2014)	Chile	0.95		4 stations (vertical channel)

Warren-Smith et al. (2018)	New Zealand	0.95	4 stations (–)	
Chaves et al. (2020)	Nicoya Peninsula, Costa Rica	0.95	Multi-station (vertical channel)	Network-averaged CC
Nadeau et al. (1995)	Parkfield, California	0.98		
Nadeau and McEvilly (1999)	Parkfield, California	0.98		
Hatch et al. (2020)	Virginia, Nevada	0.98	4 stations (–)	

[a] The minimum number of stations required for a pair of events to be classified as repeaters with the CC value exceeding the threshold value. In this column, the employed channel(s) is given in the brackets if it is explicitly documented in the reference or confirmed by the author, otherwise a dash symbol "–" is denoted.

[b] For the cases using data from two or more stations, only Yao et al. (2017) and Chaves et al. (2020) calculate the CC value simultaneously across multiple stations, and then take the average. All others compute the CC value at individual stations separately and claim an event pair to be repeaters if a certain number of stations have the CC values exceeding a given CC threshold.

Table S2. A list of digital filters commonly used in identifying repeaters

Filter	References
No Filter	Warren-Smith et al. (2018)
1–20 Hz	Cannata et al. (2013); Kimura et al. (2006)
1–10 Hz	Li et al. (2007, 2011); Ma and Wu (2013); Ma et al. (2014); Cociani et al. (2010); Schmittbuhl et al. (2016)
1–8 Hz	Matsubara et al. (2005); Meng et al. (2015); Huang and Meng (2018) ; Taira et al. (2014)
0.5–5 Hz	Green and Neuberg (2006); Schaff and Richards (2004, 2011)
1–4 Hz	Igarashi et al. (2003); Igarashi (2010, 2020); Uchida et al. (2003); Matsuzawa et al. (2004); Kato et al. (2012); Meng et al. (2015); Huang and Meng (2018)

Table S3. A list of commonly assumed $\Delta\sigma$ in estimating the ERR

Stress drop	References
3 MPa	Li et al. (2007); Lengliné and Marsan (2009); Schaff and Richards (2011); Shirzaei et al. (2013); Ma et al. (2014); Mesimeri and Karakostas (2018); Huang and Meng (2018); Igarashi (2020)
5 MPa	Li et al. (2011)
10 MPa	Igarashi et al. (2003); Matsuzawa et al. (2004); Uchida and Matsuzawa (2013); Hatakeyama et al. (2017)

References

Baisch, S., Ceranna, L., & Harjes, H. P. (2008). Earthquake cluster: What can we learn from waveform similarity?. *Bulletin of the Seismological Society of America*, *98*(6), 2806-2814.

Bao, X., & Eaton, D. W. (2016). Fault activation by hydraulic fracturing in western Canada. *Science*, *354*(6318), 1406-1409.

Buurman, H., & West, M. E. (2010). Seismic precursors to volcanic explosions during the 2006 eruption of Augustine Volcano. In J. A. Power, M. L. Coombs, & J. T. Freymueller, (Eds.), *The 2006 eruption of Augustine Volcano, Alaska*, *Professional Paper* (Vol. 1769, chap. 2, pp. 41–57). Washington, DC: U.S. Geological Survey.

Buurman, H., West, M. E., & Thompson, G. (2013). The seismicity of the 2009 Redoubt eruption. *Journal of Volcanology and Geothermal Research*, *259*, 16-30.

Cannata, A., Alparone, S., & Ursino, A. (2013). Repeating volcano-tectonic earthquakes at Mt. Etna volcano (Sicily, Italy) during 1999–2009. *Gondwana research*, *24*(3-4), 1223-1236.

Cauchie, L., Lengliné, O., & Schmittbuhl, J. (2020). Seismic asperity size evolution during fluid injection: case study of the 1993 Soultz-sous-Forêts injection. *Geophysical Journal International*, *221*(2), 968-980.

Chaves, E. J., Schwartz, S. Y., & Abercrombie, R. E. (2020). Repeating earthquakes record fault weakening and healing in areas of megathrust postseismic slip. *Science advances*, *6*(32), eaaz9317.

Chen, K. H., Nadeau, R. M., & Rau, R. J. (2008). Characteristic repeating earthquakes in an arc-continent collision boundary zone: The Chihshang fault of eastern Taiwan. *Earth and Planetary Science Letters*, *276*(3-4), 262-272.

Cociani, L., Bean, C. J., Lyon-Caen, H., Pacchiani, F., & Deschamps, A. (2010). Coseismic velocity variations caused by static stress changes associated with the 2001 Mw= 4.3 Agios Ioanis earthquake in the Gulf of Corinth, Greece. *Journal of Geophysical Research: Solid Earth*, *115*(B7).

De Angelis, S., & Henton, S. M. (2011). On the feasibility of magma fracture within volcanic conduits: constraints from earthquake data and empirical modelling of magma viscosity. *Geophysical Research Letters*, *38*(19).

Green, D. N., & Neuberg, J. (2006). Waveform classification of volcanic low-frequency earthquake swarms and its implication at Soufrière Hills Volcano, Montserrat. *Journal of Volcanology and Geothermal Research*, *153*(1-2), 51-63.

Hatakeyama, N., Uchida, N., Matsuzawa, T., & Nakamura, W. (2017). Emergence and disappearance of interplate repeating earthquakes following the 2011 M9. 0 Tohoku-oki earthquake: Slip behavior transition between seismic and aseismic depending on the loading rate. *Journal of Geophysical Research: Solid Earth*, *122*(7), 5160-5180.

Hatch, R. L., Abercrombie, R. E., Ruhl, C. J., & Smith, K. D. (2020). Evidence of Aseismic and Fluid-Driven Processes in a Small Complex Seismic Swarm Near Virginia City, Nevada. *Geophysical Research Letters*, *47*(4), e2019GL085477.

Huang, H., & Meng, L. (2018). Slow unlocking processes preceding the 2015 Mw 8.4 Illapel, Chile, earthquake. *Geophysical Research Letters*, *45*(9), 3914-3922.

Huang, H., Meng, L., Bürgmann, R., Wang, W., & Wang, K. (2020). Spatio-temporal foreshock evolution of the 2019 M 6.4 and M 7.1 Ridgecrest, California earthquakes. *Earth and Planetary Science Letters*, *551*, 116582.

Igarashi, T. (2010). Spatial changes of inter-plate coupling inferred from sequences of small repeating earthquakes in Japan. *Geophysical research letters*, *37*(20).

Igarashi, T. (2020). Catalog of small repeating earthquakes for the Japanese Islands. *Earth, Planets and Space*, *72*, 1-8.

Igarashi, T., Matsuzawa, T., & Hasegawa, A. (2003). Repeating earthquakes and interplate aseismic slip in the northeastern Japan subduction zone. *Journal of Geophysical Research: Solid Earth*, *108*(B5).

Kato, A., & Igarashi, T. (2012). Regional extent of the large coseismic slip zone of the 2011 Mw 9.0 Tohoku-Oki earthquake delineated by on-fault aftershocks. *Geophysical Research Letters*, *39*(15).

Kimura, H., Kasahara, K., Igarashi, T., & Hirata, N. (2006). Repeating earthquake activities associated with the Philippine Sea plate subduction in the Kanto district, central Japan: A new plate configuration revealed by interplate aseismic slips. *Tectonophysics*, *417*(1-2), 101-118.

Kraft, T., & Deichmann, N. (2014). High-precision relocation and focal mechanism of the injection-induced seismicity at the Basel EGS. *Geothermics*, *52*, 59-73.

Lengliné, O., & Marsan, D. (2009). Inferring the coseismic and postseismic stress changes caused by the 2004 Mw= 6 Parkfield earthquake from variations of recurrence times of microearthquakes. *Journal of Geophysical Research: Solid Earth*, *114*(B10).

Li, L., Niu, F., Chen, Q. F., Su, J., & He, J. (2017). Post-seismic velocity changes along the 2008 M 7.9 Wenchuan earthquake rupture zone revealed by S coda of repeating events. *Geophysical Journal International*, *208*(2), 1237-1249.

Ma, S. (2010). Focal depth determination for moderate and small earthquakes by modeling regional depth phases sPg, sPmP, and sPn. *Bulletin of the Seismological Society of America*, *100*(3), 1073-1088.

Ma, S., & Atkinson, G. M. (2006). Focal depths for small to moderate earthquakes (m N≥ 2.8) in Western Quebec, Southern Ontario, and Northern New York. *Bulletin of the Seismological Society of America*, *96*(2), 609-623.

Ma, X. J., & Wu, Z. L. (2013). 'Negative repeating doublets' in an aftershock sequence. *Earth, Planets and Space*, *65*(8), 923-927.

Ma, X., Wu, Z., & Jiang, C. (2014). 'Repeating earthquakes' associated with the WFSD-1 drilling site. *Tectonophysics*, *619*, 44-50.

Matsubara, M., Yagi, Y., & Obara, K. (2005). Plate boundary slip associated with the 2003 Off-Tokachi earthquake based on small repeating earthquake data. *Geophysical Research Letters*, *32*(8).

Matsuzawa, T., Uchida, N., Igarashi, T., Okada, T., & Hasegawa, A. (2004). Repeating earthquakes and quasi-static slip on the plate boundary east off northern Honshu, Japan. *Earth, planets and space*, *56*(8), 803-811.

Meng, L., Huang, H., Bürgmann, R., Ampuero, J. P., & Strader, A. (2015). Dual megathrust slip behaviors of the 2014 Iquique earthquake sequence. *Earth and Planetary Science Letters*, *411*, 177-187.

Mesimeri, M., & Karakostas, V. (2018). Repeating earthquakes in western Corinth Gulf (Greece): implications for aseismic slip near locked faults. *Geophysical Journal International*, *215*(1), 659-676.

Myhill, R., McKenzie, D., & Priestley, K. (2011). The distribution of earthquake multiplets beneath the southwest Pacific. *Earth and Planetary Science Letters*, *301*(1-2), 87-97.

Nadeau, R. M., & McEvilly, T. V. (1999). Fault slip rates at depth from recurrence intervals of repeating microearthquakes. *Science*, *285*(5428), 718-721.

Nadeau, R. M., & McEvilly, T. V. (2004). Periodic pulsing of characteristic microearthquakes on the San Andreas fault. *Science*, *303*(5655), 220-222.

Nadeau, R. M., Foxall, W., & McEvilly, T. V. (1995). Clustering and periodic recurrence of microearthquakes on the San Andreas fault at Parkfield, California. *Science*, *267*(5197), 503-507.

Naoi, M., Nakatani, M., Igarashi, T., Otsuki, K., Yabe, Y., Kgarume, T., ... & Moriya, H. (2015). Unexpectedly frequent occurrence of very small repeating earthquakes ($-5.1 \leq MW \leq -3.6$) in a South African gold mine: implications for monitoring intraplate faults. *Journal of Geophysical Research: Solid Earth*, *120*(12), 8478-8493.

Nishikawa, T., & Ide, S. (2018). Recurring slow slip events and earthquake nucleation in the source region of the M 7 Ibaraki-Oki earthquakes revealed by earthquake swarm and foreshock activity. *Journal of Geophysical Research: Solid Earth*, *123*(9), 7950-7968.

Obana, K., Kodaira, S., Kaneda, Y., Mochizuki, K., Shinohara, M., & Suyehiro, K. (2003). Microseismicity at the seaward updip limit of the western Nankai Trough seismogenic zone. *Journal of Geophysical Research: Solid Earth*, *108*(B10).

Peng, Z., & Ben-Zion, Y. (2005). Spatiotemporal variations of crustal anisotropy from similar events in aftershocks of the 1999 M 7.4 Izmit and M 7.1 Düzce, Turkey, earthquake sequences. *Geophysical Journal International*, *160*(3), 1027-1043.

Petersen, T. (2007). Swarms of repeating long-period earthquakes at Shishaldin Volcano, Alaska, 2001–2004. *Journal of Volcanology and Geothermal Research*, *166*(3-4), 177-192.

Rau, R. J., Chen, K. H., & Ching, K. E. (2007). Repeating earthquakes and seismic potential along the northern Longitudinal Valley fault of eastern Taiwan. *Geophysical research letters*, *34*(24).

Robinson, D. J., Sambridge, M., & Snieder, R. (2011). A probabilistic approach for estimating the separation between a pair of earthquakes directly from their coda waves. *Journal of Geophysical Research: Solid Earth*, *116*(B4).

Salvage, R. O., & Neuberg, J. W. (2016). Using a cross correlation technique to refine the accuracy of the Failure Forecast Method: Application to Soufrière Hills volcano, Montserrat. *Journal of Volcanology and Geothermal Research*, *324*, 118-133.

Schmittbuhl, J., Karabulut, H., Lengliné, O., & Bouchon, M. (2016). Long-lasting seismic repeaters in the Central basin of the Main Marmara fault. *Geophysical Research Letters*, *43*(18), 9527-9534.

Schultz, R., Stern, V., & Gu, Y. J. (2014). An investigation of seismicity clustered near the Cordel Field, west central Alberta, and its relation to a nearby disposal well. *Journal of Geophysical Research: Solid Earth*, *119*(4), 3410-3423.

Schultz, R., Wang, R., Gu, Y. J., Haug, K., & Atkinson, G. (2017). A seismological overview of the induced earthquakes in the Duvernay play near Fox Creek, Alberta. *Journal of Geophysical Research: Solid Earth*, *122*(1), 492-505.

Shearer, P. M. (1997). Improving local earthquake locations using the L1 norm and waveform cross correlation: Application to the Whittier Narrows, California, aftershock sequence. *Journal of Geophysical Research: Solid Earth*, *102*(B4), 8269-8283.

Shearer, P. M. (2009). *Introduction to seismology*. Cambridge university press.

Shirzaei, M., Bürgmann, R., & Taira, T. A. (2013). Implications of recent asperity failures and aseismic creep for time-dependent earthquake hazard on the Hayward fault. *Earth and Planetary Science Letters*, *371*, 59-66.

Snieder, R., & Vrijlandt, M. (2005). Constraining the source separation with coda wave interferometry: Theory and application to earthquake doublets in the Hayward fault, California. *Journal of Geophysical Research: Solid Earth*, *110*(B4).

Taira, T. A., Bürgmann, R., Nadeau, R. M., & Dreger, D. S. (2014). Variability of fault slip behavior along the San Andreas Fault in the San Juan Bautista Region. *Journal of Geophysical Research: Solid Earth*, *119*(12), 8827-8844.

Thelen, W., Malone, S., & West, M. (2011). Multiplets: Their behavior and utility at dacitic and andesitic volcanic centers. *Journal of Geophysical Research: Solid Earth*, *116*(B8).

Thelen, W., West, M., & Senyukov, S. (2010). Seismic characterization of the fall 2007 eruptive sequence at Bezymianny Volcano, Russia. *Journal of Volcanology and Geothermal Research*, *194*(4), 201-213.

Trugman, D. T., & Shearer, P. M. (2017). GrowClust: A hierarchical clustering algorithm for relative earthquake relocation, with application to the Spanish Springs and

Sheldon, Nevada, earthquake sequences. *Seismological Research Letters*, *88*(2A), 379-391.

Uchida, N., & Matsuzawa, T. (2013). Pre-and postseismic slow slip surrounding the 2011 Tohoku-oki earthquake rupture. *Earth and Planetary Science Letters*, *374*, 81-91.

Uchida, N., Matsuzawa, T., Hasegawa, A., & Igarashi, T. (2003). Interplate quasi-static slip off Sanriku, NE Japan, estimated from repeating earthquakes. *Geophysical Research Letters*, *30*(15).

Wang, R., Gu, Y. J., Schultz, R., Zhang, M., & Kim, A. (2017). Source characteristics and geological implications of the January 2016 induced earthquake swarm near Crooked Lake, Alberta. *Geophysical Journal International*, *210*(2), 979-988.

Warren-Smith, E., Fry, B., Kaneko, Y., & Chamberlain, C. J. (2018). Foreshocks and delayed triggering of the 2016 MW7. 1 Te Araroa earthquake and dynamic reinvigoration of its aftershock sequence by the MW7. 8 Kaikōura earthquake, New Zealand. *Earth and Planetary Science Letters*, *482*, 265-276.

Yamaguchi, J., Naoi, M., Nakatani, M., Moriya, H., Igarashi, T., Murakami, O., ... & Ogasawara, H. (2018). Emergence and disappearance of very small repeating earthquakes on a geological fault in a gold mine in South Africa. *Tectonophysics*, *747*, 318-326.

Yamashita, Y., Shimizu, H., & Goto, K. (2012). Small repeating earthquake activity, interplate quasi-static slip, and interplate coupling in the Hyuga-nada, southwestern Japan subduction zone. *Geophysical research letters*, *39*(8).

Zhang, J., Song, X., Li, Y., Richards, P. G., Sun, X., & Waldhauser, F. (2005). Inner core differential motion confirmed by earthquake waveform doublets. *Science*, *309*(5739), 1357-1360.

Zhao, P., & Zhigang, P. (2009). Depth extent of damage zones around the central Calaveras fault from waveform analysis of repeating earthquakes. *Geophysical Journal International*, *179*(3), 1817-1830.